

Structural, electronic and magnetic properties of Fe doped CoCr_2O_4 : insights from ab initio calculations

Debashish Das,¹ Shreemoyee Ganguly,² Biplab Sanyal,³ and Subhradip Ghosh¹

¹*Department of Physics, Indian Institute of Technology Guwahati, Guwahati, Assam 781039, India*

²*S.N.Bose National Center for Basic Sciences, JD Block Sector III, Salt Lake City, Kolkata 700098, India*

³*Department of Physics and Astronomy, Uppsala University, Box 516, 75120 Uppsala, Sweden**

(Dated: June 14, 2016)

CoCr_2O_4 has attracted significant attention recently due to several interesting properties such as magnetostriction, magnetoelectricity etc.. More recent experiments on Fe substituted CoCr_2O_4 observed a variety of novel phenomena such as the magnetic compensation accompanied by the occurrence of exchange bias, which reverses its sign. Understanding of such phenomena may lead to control the properties of these material in an efficient way to enhance its potential for multifunctional applications. In this paper, we study the microscopic understanding of Fe doping in modifying the structural and magnetic properties of CoCr_2O_4 with varying composition and substitution of Fe at different sublattices by first-principles density functional calculations. We have analysed in detail the effect of Fe substitution on crystal field and exchange splittings, magnetic moments and interatomic exchange parameters. It is also observed that with increasing concentration of Fe impurity, the system has a tendency towards forming an "Inverse Spinel" structure as observed in experiments. Such tendencies are crucial to understand this system as it would lead to modifications in the magnetic exchange interactions associated with sites with different symmetry finally affecting the magnetic structure and the multiferrocity in turn.

I. INTRODUCTION

CoCr_2O_4 , a member of the spinel oxide family, has received considerable attention in past few years after the discovery of magnetisation reversal of ferroelectric polarisation in this material¹. Subsequent studies, in order to explore the multiferroic nature of this system, resulted in illuminating temperature and magnetic field dependent magnetocaloric properties^{2,3}. This material has a rich magnetic phase diagram. At a temperature around 93 K, it exhibits a collinear ferromagnetic ordering followed by a transformation to a complex incommensurate conical spin spiral around 26 K^{4,5}. This conical spin spiral further transforms to a commensurate one⁶, which further undergoes unconventional magneto-structural transitions at high magnetic fields^{7,8}. The origin of ferroelectric polarisation in this material is believed to be due to the conical spin spiral state and is explained by the inverse Dzyaloshinskii-Moriya effect¹.

CoCr_2O_4 crystallises in normal spinel structure in which the Co^{2+} ions occupy the A sites having tetrahedral symmetry and the Cr^{3+} ions occupy the B sites with octahedral symmetry. The magnetoelectric coupling in this material is attributed to the conical order of the Cr^{3+} sublattice¹. This very well fits into the so called LKDM theory⁹ which, by using a simple Heisenberg model, demonstrates that the magnetic exchange interactions among A-B and B-B ions determine the magnetic order in cubic spinels. However, recent measurements^{6,10} and first-principles electronic structure calculations¹¹ establish that the magnetic structure at the A site and the magnetic exchange interactions among A ions cannot be neglected at low temperatures. Therefore, the variations in the occupancies at the A and B sub-lattices can induce significant changes in the magnetic interactions, thus in-

fluencing the magnetic order and the associated electric polarisation.

It is, thus, interesting to investigate the effects of substitutions by a third magnetic cation in CoCr_2O_4 , as that might affect the magnetic exchange interactions, thereby affecting the stabilities of the spin spiral states leading to interesting functional properties. To this end, recent attempts on Fe substitution at the B sublattice have been remarkable. Magnetic measurements on $\text{Co}(\text{Cr}_{0.95}\text{Fe}_{0.05})_2\text{O}_4$ ¹² and on $\text{Co}(\text{Cr}_{0.925}\text{Fe}_{0.075})_2\text{O}_4$ ¹³ show the phenomenon of magnetic compensation and sign reversal of Exchange Bias¹⁴ around a critical temperature. These unusual phenomena vanish when Fe content reaches about 12.5% in the B sublattice. These effects were attributed to the spin reorientations of the magnetic cations at various sublattices^{12,15}. This point was further elucidated by Zhang *et al*¹⁶ who upon investigations of the magnetic compensations in $\text{CoCr}_{2-x}\text{Fe}_x\text{O}_4$ systems inferred that the magnetic compensation can be understood in terms of a role conversion of magnetic contributors and a composition compensation between two competitive magnetic sublattices at $x = 0.1$, the origin of which is the changes in the sublattice occupancies of the Fe^{3+} ions. They also found a significant magnetostriction at $x = 0.4$, which is consistent with the composition and temperature dependent compensation behaviour.

These experimental results demonstrate that the understanding of the competitive roles of the magnetic components at various sublattices is the key to comprehend the fascinating physics exhibited by Fe substituted CoCr_2O_4 . Some of us have recently studied¹⁷ the evolution of magnetic and electronic structures in CoCr_2O_4 while going from 'normal spinel' to 'inverse spinel' by Fe doping. However, the structural aspects and their connection to electronic and magnetic structures was not

considered in that study. In this communication, we, report density functional theory (DFT) based calculations on the structural, electronic and magnetic properties of Fe doped CoCr_2O_4 with a specific focus on doping at different sublattices. Our results throw light on the fundamental aspects of structural deformations, the comparative roles of crystal field and magnetic exchange fields, the electronic correlations, doping at different sublattices and the hybridisations due to Fe substitution in CoCr_2O_4 . These results can help in microscopic understanding of the physical interactions in this system. The paper is organised as follows: Section II details the methodology used, section III is dedicated to the results and discussions followed by the conclusions.

II. METHODOLOGY

CoCr_2O_4 crystallises in the spinel structure with space group $Fd\bar{3}m$. The structure can be described as an approximately close-packed arrangement of oxygen anions with metal cations distributed amongst the tetrahedral and octahedral sites in A and B sublattices respectively. The eightfold positions ($000 : \frac{1}{4} \frac{1}{4} \frac{1}{4}$) are the tetrahedral sites occupied by the Co^{2+} cations, while the sixteen fold positions ($\frac{5}{8} \frac{5}{8} \frac{5}{8} : \frac{5}{8} \frac{7}{8} \frac{7}{8} : \frac{7}{8} \frac{5}{8} \frac{7}{8} : \frac{7}{8} \frac{7}{8} \frac{5}{8}$) are the octahedral sites occupied by the Cr^{3+} cations. The oxygen anion sublattice is arranged in a pseudo-cubic close packed spatial arrangement. A 14 atom unit cell (2 formula units) with $Fd\bar{3}m$ symmetry is considered for pristine CoCr_2O_4 in the present calculations. Collinear Neel configuration is considered as the magnetic structure where all Cr spins are parallel to each other but are antiparallel to the Co spins. To model Fe substituted CoCr_2O_4 we have considered a $2 \times 2 \times 2$ supercell of the 14 atom primitive cell consisting of 112 atoms. We have investigated the systematic effects of Fe doping by first replacing one Cr atom and then two Cr atoms. Substitution of one Cr atom leads to $\text{Co}(\text{Cr}_{1-x}\text{Fe}_x)_2\text{O}_4$ with $x \sim 0.03125$ amounting to 6.25 % Fe content at B sites, while substitution of two Cr atoms lead to the case with $x \sim 0.0625$ amounting to 12.5 % Fe content at B sites. It is to be noted that these x values are close to $x = 0.05$ where the phenomena like magnetic compensation, negative magnetisation and reversible EB effect have been observed¹².

The total energies, structural parameters, electronic structure and magnetic properties are calculated by DFT+U¹⁹ method. Inclusion of the effects of strong correlations is a necessity for oxides²⁰⁻²³ and one of the simplest methods is to use DFT+U. Also, it was shown¹¹ that non-incorporation of correlation effects lead to wrong ground state for CoCr_2O_4 . In this work, we have used the DFT+U approach adopted by Dudarev *et al*²⁴. In this approach, the effect of correlation is addressed through the effective Hubbard parameter $U_{eff} = U - J$, where U denotes the strength of the Coulomb interaction, the so called "Hubbard U " and J is the intra-atomic Hund's parameter. We have used 5 eV for U_{Co} , 3

eV for U_{Cr} and 4 eV for U_{Fe} . The value of J was taken to be 1 eV for all the elements. Such choices were based upon the available information^{11,25-27}. We have used the Projector Augmented Wave (PAW)²⁹ formalism as implemented in VASP code³⁰. The exchange-correlation part of the Hamiltonian was treated with PBE-GGA functional³¹. A plane wave cut-off energy of 400 eV was considered for all the cases. The positions of all atoms were relaxed keeping the volume fixed at the experimental one. The relaxations were carried out till the forces are less than 10^{-3} eV/Å. The electronic self-consistency cycle is iterated till the total energy is converged better than 10^{-5} eV. A $2 \times 2 \times 2$ Γ centred k -mesh was used for self-consistency and a $5 \times 5 \times 5$ mesh was used for calculations of the electronic structure.

The structural distortions in the compounds are assessed by computing angles θ_{Td} and θ_{Oh} , which denote the distortions from perfect tetrahedral and octahedral symmetries respectively, and are defined as,

$$\theta_{Td} = \sum_{i=1}^4 \frac{|109.5 - \theta_i^{Td}|}{n}$$

$$\theta_{Oh} = \sum_{i=1}^8 \frac{|90 - \theta_i^{Oh}|}{n} \quad (1)$$

$\theta_i^{Td}, \theta_i^{Oh}$ are the ligand-metal-ligand bond angles corresponding to the i -th bond for the tetrahedral and octahedral symmetries respectively.

The magnetic properties are investigated by computing the total and partial magnetic moments and the magnetic exchange parameters. To determine the magnetic exchange parameters J_{ij} among sub-lattices i, j , we have calculated total energies for different collinear magnetic configurations and mapped them onto a classical Heisenberg Hamiltonian

$$E = - \sum_{i,j} J_{ij} \vec{S}_i \cdot \vec{S}_j$$

where S_i and S_j are the unit spin vectors. It should be noted that $J_{ij} > 0$ (< 0) denotes ferromagnetic (antiferromagnetic) coupling.

III. RESULTS AND DISCUSSIONS

A. Pristine CoCr_2O_4

Before embarking on the effect of Fe doping, the pristine CoCr_2O_4 is investigated, in particular the structural aspects. We have done calculations at the experimental lattice constant of 8.335 Å³² and optimised the internal structure parameter u , which corresponds to the oxygen sites. Our calculated value of u is 0.261, which agrees very well with the earlier results^{11,32}. As was mentioned earlier, the magnetic configuration considered is the collinear Neel configuration. We have considered the Cr magnetic moments to be "spin up" and the Co moments to be "spin down". Our calculations showed both

Co and Cr in high spin states with magnetic moments - $2.66 \mu_B$ and $2.93 \mu_B$ respectively, resulting in a magnetic moment of about $3 \mu_B$ per formula unit for the system.

In Fig. 1 we show a part of the neighbourhood of the octahedrally coordinated Cr and tetrahedrally coordinated Co atom. All the relevant angles and bond lengths are also demonstrated. In order to assess the structural distortions in this compound, we have estimated the values of angles θ_{T_d} and θ_{O_h} in accordance with Eqn.(1). While $\theta_{T_d} \sim 0.03^\circ$ [the angles vary between 102.56° and 109.48°], $\theta_{O_h} \sim 5.34^\circ$ [the angles vary between 84.67 and 95.34]. The results suggest that the distortions associated with the tetrahedral sites are negligible.

B. $\text{Co}(\text{Cr}_{0.96875}\text{Fe}_{0.03125})_2\text{O}_4$

We have mentioned earlier that the above composition is modelled by replacing one Cr atom by an Fe atom in the 112 atom cell. This Fe atom can occupy a B site or can occupy an A site. In the later case, it will displace one Co atom which will occupy the B site, vacant due to replacement of Cr. This substitution by Fe at A site mimics the tendency towards formation of "Inverse" structure, where in the case of an AB_2O_4 compound, one B atom will occupy the tetrahedral site, pushing the lone A atom to the octahedral site. The case of Fe substitution at A site is particularly interesting as it now provides us with, apart from the substituting impurity at A site, the presence of Co atoms at both tetrahedral and octahedral sites. The resulting effects on the structural distortions, the spin structure of the system and the electronic structure would throw some light on the microscopic physics in the system which would become more relevant at higher Fe concentrations where the inversion indeed starts to occur¹⁶. In the following sub-sections we report results on both substitution at A site and at B site.

1. Fe substitution at A site

We first report the minimum energy spin configuration for a single Fe atom substituting a Co at site A. In order to find this, we have considered three different bond distances between Co at tetrahedral sites(Co_T) and Co at octahedral sites(Co_O). For each of the three distances, we have calculated total energies of different spin orientations of atoms at A and at B sites to obtain the minimum energy spin configuration. The results are summarised in Table I. Our results show that the Co atoms at tetrahedral and at octahedral sites prefer to be nearest neighbours, the spins of substituted Fe, and the Co at octahedral as well as as tetrahedral sites prefer to align anti-parallel to the spin of the Cr atom. The results of magnetisation show that the substituted Fe atom is in a high spin state; so are the other atoms. The magnetic moments of Co at tetrahedral site, the Co at octahedral

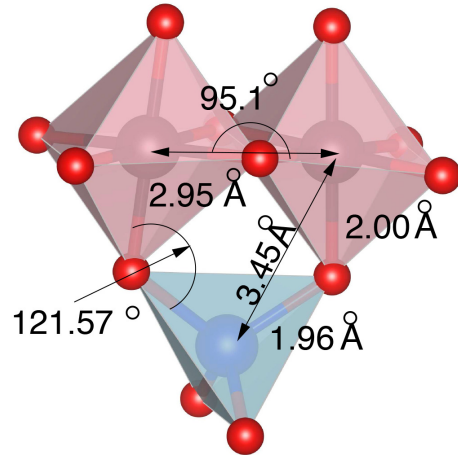


FIG. 1. A part of near neighbourhood of the tetrahedrally coordinated Co atom and octahedrally coordinated Cr atom in pristine CoCr_2O_4 is shown. Various bond angles and bond lengths are shown. The Co atoms are shaded blue, the Cr atoms pink and the O atoms red.

TABLE I. Total energy (meV) per Fe atom and the spin structure for different bond distances between Co at tetrahedral site (Co_T) and Co at octahedral site (Co_O) for Fe substitution at A site in CoCr_2O_4 .

Co _T -Co _O bond distance (Å)	Orientation of spins				Total energy
	Co _T	Co _O	Cr	Fe	
3.45	↓	↓	↑	↓	0
5.4	↓	↑	↑	↓	46
6.87	↓	↑	↑	↓	87

site, the Fe and the Cr are $-2.66 \mu_B$, $-2.71 \mu_B$, $-4.02 \mu_B$ and $2.93 \mu_B$ respectively, yielding a total magnetic moment of about $2.5 \mu_B$ per formula unit. Thus, the moment of Co atoms remain almost constant with respect to those in pristine CoCr_2O_4 and the reduction in the overall moment is due to the large anti-parallel moment of Fe.

After fixing the minimum energy spin configuration, we analyse the structural parameters and the electronic structure. Since the lattice constant and oxygen u parameter do not change appreciably for such a low concentration of Fe substitution¹⁶, we have kept them the same as those of CoCr_2O_4 and relaxed the atom positions only. It is observed that the oxygen atoms in the Co octahedra move outwards while those in the Fe tetrahedra move inwards resulting in slight contractions in the substituted tetrahedra and slight expansions in the substituted octahedra. This can be understood from the fact that the size of Co is larger than that of Cr and Fe. So, when the Co atom is substituted at an octahedral site, it expands the octahedra locally while the Fe that substitutes a Co at tetrahedral site contracts the tetrahedra.

In Fig. 2, we show the neighbourhood of the substituted transition metals along with the relevant structural parameters. Upon Fe substitution at A site, the Fe-O-Cr and the Fe-O-Co_O angles increase and decrease respectively in comparison to the Co-O-Cr angle in CoCr₂O₄ quantifying the distortions around the substituted sites. The values of θ_{T_d} and θ_{O_h} [calculated using Eqn. (1)] are $\sim 0.71^\circ$ [the angles vary between $108.36^\circ - 112.32^\circ$] and 5.95° [the angles vary between $83.80^\circ - 96.95^\circ$] respectively. This implies that the distortion in the tetrahedral environment is more due to Fe substitution at tetrahedral sites. These results indicate that the degeneracies in the d orbitals of the transition metal atoms are going to be affected and one can expect a significant impact on the electronic structure.

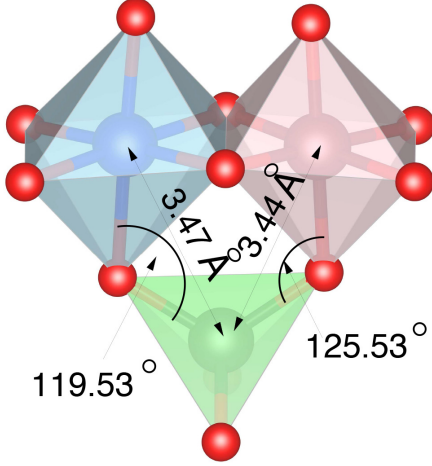


FIG. 2. A part of near neighbourhood of the tetrahedrally coordinated *Fe* atom and octahedrally coordinated *Co* atom are shown along with various bond angles and bond lengths for single Fe substituted at A site in CoCr₂O₄. The Co atoms are shaded blue, the Fe atoms green, the Cr atoms pink and the O atoms red.

In what follows, we provide an understanding of the effects of structural distortion and electron-electron correlation on the electronic structure and individual spin states of the constituents by a study of the crystal field splitting (CF) and exchange splitting (Ex) through an analysis of the corresponding densities of states. Before analysing the Fe substituted system, we first look at the pristine compound. The exchange splitting of t_{2g} and e_g levels and the crystal field splitting of the spin channels for Co and Cr occupying A and B sites respectively are listed in the first two rows of Table II. These results are obtained without the effects of correlations, that is, for $U = 0$. The results suggest that in the down spin channel (\downarrow) of A site, the five-fold 3d crystal field degeneracy is barely broken. Thus, this spin band is almost completely occupied resulting in a high spin state for Co cation. The other 3d electrons mostly occupy the exchange split ($\Delta_{EX}^{e_g} = 1.5$ eV) e_g up spin channel (\uparrow). The t_{2g}^{\uparrow} states being energetically much higher ($\Delta_{EX}^{t_{2g}} = 2.7$ eV) remains

unoccupied. For the B site, the triply degenerate t_{2g}^{\uparrow} states are energetically much lower than the corresponding e_g^{\uparrow} ($\Delta_{CF}^{\uparrow} = 3.2$ eV) and t_{2g}^{\downarrow} ($\Delta_{EX}^{t_{2g}} = 3.2$ eV). Thus these (t_{2g}^{\uparrow}) states are almost completely occupied resulting in a high spin state of Cr. The energy level diagram of Figure 3(i) sums it up. Upon substitution by Fe at A

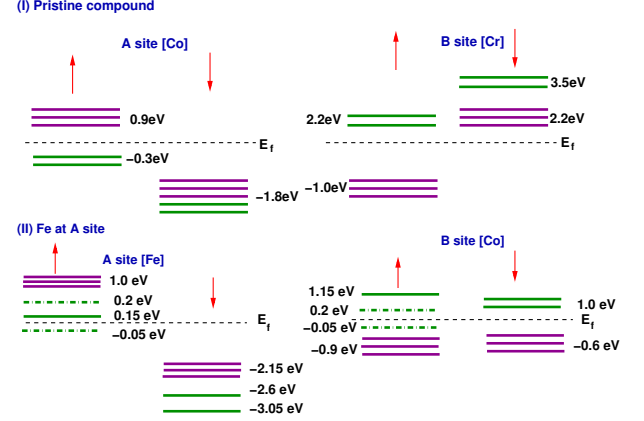


FIG. 3. (i) The crystal field and exchange splitting of the t_{2g} (d_{xy}, d_{yz} and d_{xz}) and e_g (d_{z^2} and $d_{x^2-y^2}$) levels of pristine CoCr₂O₄ are analysed through Energy Level Diagram. While the t_{2g}^{\downarrow} , e_g^{\downarrow} and e_g^{\uparrow} are almost completely occupied for the tetrahedrally coordinated A site, only the t_{2g}^{\uparrow} levels are primarily occupied for the B site. (ii) The crystal field and exchange splitting of the t_{2g} (d_{xy}, d_{yz} and d_{xz}) and e_g (d_{z^2} and $d_{x^2-y^2}$) levels of Fe substituted (at A site) CoCr₂O₄ are analysed through Energy Level Diagram. The level splitting of only the substituted atoms (Fe for A site and Co_O for B site) are shown. The t_{2g} levels are marked purple and the e_g levels are marked green.

site, the exchange and crystal field splitting of the parent atoms (Co_T at A and Cr at B site) located in the far neighbourhood of the sites of substitutions remain much like the ones of the pristine compound. In the near neighbourhood of the substituted sites, the densities of states show traces of broken degeneracy (Not shown here). This must be the effect of structural distortion. Of particular interest in this context is the densities of states for the displaced Co atom at B site (Co_O). The d_{z^2} \uparrow level for this atom overlaps with the corresponding d_{z^2} level of the Fe atom at A site as shown in Figure 4. As a result the levels show splitting about the Fermi level. This indicates that the Fe-Co_O d_{z^2} orbitals hybridise to form molecular orbitals. These split states are represented by the broken lines in the energy level diagram Figure 3(ii). It is interesting to note that the degeneracy in the e_g states present in the down (\downarrow) spin channel of the pristine compound (due to T_d symmetry) is broken due to Fe substitution. This was already indicated by the increase in θ_{T_d} . The non-degenerate states, formed, overlap with the corresponding oxygen p states as expected. The exchange splitting at the A sites for both e_g and t_{2g} levels increases due to Fe substitution as is seen from 3rd row of Table II. This ensures that not more than one elec-

tronic state of the substituted atom is occupied in the minority spin channel. However the Co atom displaced to the octahedral site has a much lower exchange splitting resulting the Co_o to be in a low spin state. Inclusion

TABLE II. Substituted site (\mathcal{A} and \mathcal{B}), Exchange Splitting of e_g and t_{2g} levels ($\Delta_{EX}^{e_g}$ and $\Delta_{EX}^{t_{2g}}$ respectively) and Crystal Field Splitting of up and down spin channels (Δ_{CF}^\uparrow and Δ_{CF}^\downarrow respectively) for different Species (the first two rows are for parent compound where Co atom is at \mathcal{A} site and Cr atom at \mathcal{B} , next two rows are for the substituted Fe at \mathcal{A} site and the Co_o atom at \mathcal{B} site; the last row is for substituted Fe at \mathcal{B} site).

Site	Species	$\Delta_{EX}^{e_g}$ (eV)	$\Delta_{EX}^{t_{2g}}$ (eV)	Δ_{CF}^\uparrow (eV)	Δ_{CF}^\downarrow (eV)
\mathcal{A}	Co	1.50	2.70	1.20	0.0
\mathcal{B}	Cr	1.30	3.20	3.20	1.3
\mathcal{A}	Fe	2.93	3.15	0.9	0.68
\mathcal{B}	Co	0.57	0.3	1.33	1.6
\mathcal{B}	Fe	2.85	3.55	2.5	1.8

of the electron-electron correlation through the Coulomb parameter U brings in drastic changes in the densities of states and subsequently in the exchange splitting. A high spin state of the displaced Co at B site emerges with a magnetic moment about $3 \mu_B$ similar to the value at the original tetrahedral site. Moreover, the direction of the magnetic moment of this displaced Co is aligned with the Fe moment (Table I), which was anti-aligned in pure GGA calculations (Fig. 3(ii)). This indicates the failure of GGA in describing properly the electronic structure of oxides and the necessity of adding strong Coulomb interactions. In Figure 5, we compare the densities of states of the pristine and the Fe substituted (at A site) CoCr_2O_4 along with the atom projected DOSs. The results for pristine CoCr_2O_4 (Figure 5 (top)) qualitatively agree with previously published one¹¹. Upon Fe substitution, one can see significant changes in the densities of states (Figure 5 (top)). New peaks at 1 eV above Fermi level in the up (\uparrow) band, at 0.45 eV, 0.65 eV, 6.8 eV and 7.4 eV below Fermi level in the down (\downarrow) band appear. The inclusion of electron-electron correlation pushes the Co_o and Fe d_{z^2} states, which had formed molecular orbitals for $U=0$ case to higher energies. These are the new states appearing in the up band at around 1 eV above Fermi level. This leads to the correct charge states of +2 and +3 for Co_o and Fe atoms respectively. The peaks at 6.8 eV and 7.4 eV below Fermi level, in the down band, are the contributions mostly from the e_g and t_{2g} states of Fe respectively. The peak at -7.4 eV in the down band results from the hybridisation of Fe t_{2g} with Co_o e_g states via adjoining oxygen 2p states and correspond to Fe-O- Co_o superexchange. The peak at -6.8 eV in the down band, similarly, results from hybridisation of Fe t_{2g} and Co_o t_{2g} states via oxygen. The prominent peak at -6.15 eV in the down band results from hybridisations between Co_o e_g and Co_T t_{2g} via oxygen 2p states, that is, originating via Co_T -O- Co_o superexchange. The peaks

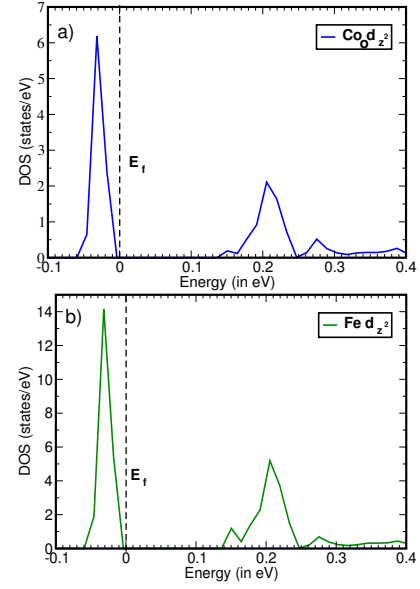


FIG. 4. The Co_o and Fe densities of states for the d_{z^2} orbitals when Fe is substituted at A site of CoCr_2O_4 . The hybridisations show formation of molecular orbitals. The calculations are for $U_{eff} = 0$.

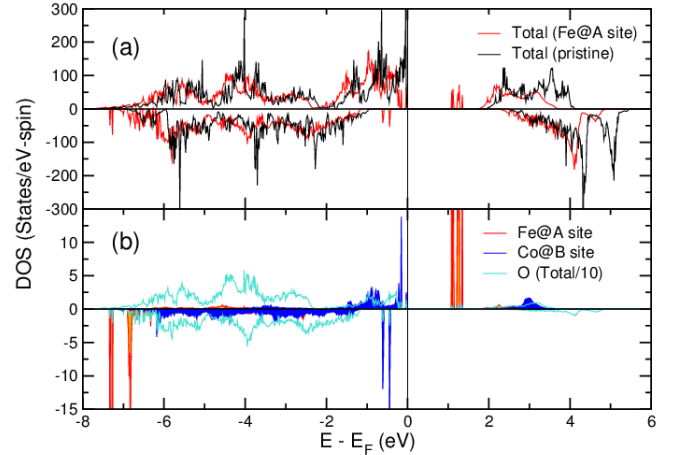


FIG. 5. (top) Total densities of states for pristine CoCr_2O_4 and for a single Fe substituted at A site in CoCr_2O_4 . (bottom) The atom projected densities of states for Fe, Co_o and oxygen atoms for single Fe substituted at A site in CoCr_2O_4 .

at -0.45 eV and -0.65 eV in the down band arises solely due to Co_o e_g states arising due to electron-electron correlation. Such re-distribution of states increases the exchange splitting at Co_o site and helps to achieve the high spin state.

2. Fe substitution at B site

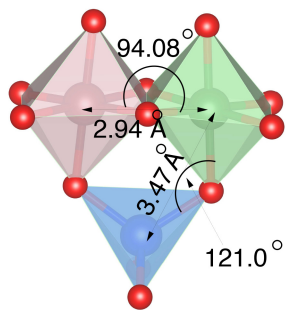


FIG. 6. A part of near neighbourhood of the octahedrally coordinated *Fe* atom is shown along with various bond angles and bond lengths for single Fe substituted at B site in CoCr_2O_4 . The Co atoms are shaded blue, the Fe atoms green, the Cr atoms pink and the O atoms red.

The Fe moments prefer to align anti-parallel to those of Cr when Fe is substituted at B site. The total energy of this configuration is lower by an amount of 413 meV per Fe atom than the minimum energy configuration in case of Fe substitution at A site. Thus, for this concentration of Fe substitution, the B site substitution is preferred and the system is a normal spinel. This is in agreement with the experimental observation¹⁶ that the inversion starts occurring for $x > 0.05$. In this case too, all the magnetic components are in high spin states and the individual moments do not change from those in the case of substitution at A site. In Figure 6, we show the

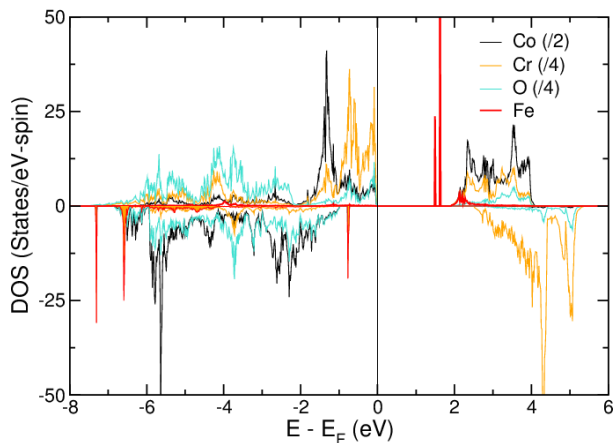


FIG. 7. Atom projected densities of states for a single *Fe* substituted at B sublattice in CoCr_2O_4 .

structural distortions around the Fe site and the relevant structural parameters along with the overall deviations from the octahedral symmetry due to Fe substitution at the octahedral site. It is observed that the octahedron

around Fe expands, the reason being the substitution of Cr by an atom of larger size. The deviation from the octahedral symmetry is almost same as that in case of the pristine compound as is seen by comparing θ_{O_h} ($\sim 5.34^\circ$ for the pristine compound, while $\sim 5.27^\circ$ for Fe impurity site in the doped compound) in both cases. The Fe-O-Co and Fe-O-Cr angles remain almost at the values of the Co-O-Cr and Cr-O-Cr angles in pristine compound. Even the bond lengths change only slightly from those in the CoCr_2O_4 . Thus we do not expect to see changes in the electronic structure as substantial (in comparison with CoCr_2O_4) as was observed in case of substitution at A site.

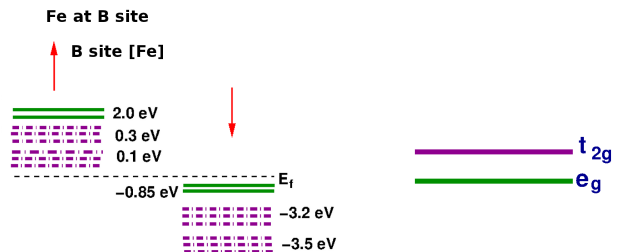


FIG. 8. The energy level diagram showing the crystal field and exchange splitting of the t_{2g} and e_g levels of Fe substituted at B site. The t_{2g} levels are marked purple and the e_g levels are marked green.

The last row of Table II lists the crystal field splitting and exchange splitting for the substitution at B site (without including the effect of electron-electron correlation). Unlike Co substitution at B site, substitution by Fe enhances the exchange splitting of e_g and t_{2g} levels. This ensures that not more than one electronic state of the substitute is occupied in the minority spin channel. Thus, it appears that the Fe spin state is unaffected by the symmetry of the site where it is substituted into. In order to understand the impact on the electronic structure, we once again take recourse to the energy level diagram for the Fe atom in Figure 8. Although the deviations from the O_h symmetry is same as that of the CoCr_2O_4 , both the Fe t_{2g}^\uparrow and t_{2g}^\downarrow levels show splitting. These split states are shown by broken lines in Figure 8. These split levels overlap with the adjoining oxygen. Interestingly, the 3-fold and 2-fold degeneracy of the t_{2g} and e_g states, respectively, is maintained at B site even after Fe substitution. In the distant neighbourhood of Fe sites, the situations for Co atoms at A site and Cr atoms at B sites remain quite similar to that of the pristine CoCr_2O_4 . In the nearest neighbourhood of Fe site, there are 6 octahedrally and 6 tetrahedrally coordinated sites. Both these sites show reduced symmetry due to Fe substitution and as a result there is a slight loss of degeneracy in the t_{2g} states.

Figure 7 shows the DOSs for a single Fe atom sub-

stituted at a B site. It is observed that the inclusion of the electron-electron correlation affects the densities of states of Fe, with prominent effects on the t_{2g} states. The split t_{2g}^{\uparrow} states near the Fermi level are now pushed deeper into the conduction band while the e_g^{\uparrow} states are unaffected. Similarly the e_g^{\downarrow} states at -0.85 eV remain unaffected. The electron electron correlation pushes the split t_{2g}^{\downarrow} bands deeper into the valence band at -7.25 eV. However, the peaks in the total densities of states are not due to Fe alone. The peak at -7.25 eV in the down band arises out of hybridisation of Fe t_{2g} and Co e_g orbitals through oxygen 2p. The two peaks at -0.85 eV and -6.5 eV arises out of hybridisations of Fe e_g with Co t_{2g} through oxygen 2p. The peak at -3.9 eV arises out of hybridisation of Fe and Cr e_g orbitals, once again via oxygen p orbitals.

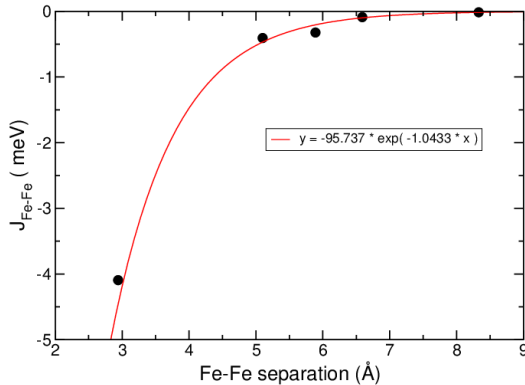


FIG. 9. Interatomic exchange interactions between Fe atoms substituted at B sublattice as a function of Fe-Fe distance. The data points have been fitted (shown as a red line) with an exponential function as shown in the figure.

Thus, we see that the effects of Fe substitution at B site is less dramatic than that at A site. The impact of local structural distortion is more severe on the electronic structure of Fe substituted CoCr_2O_4 at A site. For the case of Fe substitution at A site, the two Co atoms having different symmetry associated with their sites, bring in additional dimensions to the impact of substitutions. It is, therefore, expected that the exchange interactions associated with the A site and B sites would be quite different depending upon the site of Fe substitution. This, in turn, would affect the LKDM parameter u and subsequently the occurrence of non collinear states.

C. $\text{Co}(\text{Cr}_{0.9375}\text{Fe}_{0.0625})_2\text{O}_4$

In a 112 atom cell, this composition is modelled by replacing two Cr atoms by two Fe atoms. The distance between two Fe atoms can be 2.78, 5.1, 5.89, 6.83 and

8.33 Å. We found that the relative spin orientations of the constituent magnetic atoms change depending upon the Fe-Fe distance. In Fig 9, the interatomic exchange interactions between Fe atoms are shown as a function of Fe-Fe distance. These have been obtained from total energies for minimum energy spin configurations. As seen, all the exchange interactions are antiferromagnetic in nature. This 90° antiferromagnetic superexchange interaction follows from Goodenough-Kanamori rules.³³ Also, we have found that the Fe atoms prefer to stay far away from each other and that the substituted Fe prefer to align the spins anti-parallel to the Cr spins. As expected, the exchange interactions decay exponentially with distance. This basically indicates that for a low concentration and a homogeneous distribution of Fe atoms, one should not expect a prominent contribution of exchange from Fe atoms in transition temperatures.

The above discussion is for Fe substitution at B sites. We also checked the possibilities of Fe substitution at A sites. Since substitution of both Fe atoms at A sites would mean complete inversion, we only looked into the case when one of the two Fe atoms are substituted into A sites. We found that this configuration lies at an energy 185 meV per Fe atom higher than the configuration when both Fe occupy B sites. We have earlier reported that for $x = 0.03125$, this difference is more than 400 meV per Fe atom. This result, thus, shows that as Fe concentration increases, the tendency for the Fe atoms to occupy A sites increases, in agreement with experiments¹⁶.

IV. CONCLUSIONS

Using density functional theory based calculations, we have carried out systematic investigations into the structural and magnetic properties of $\text{Co}(\text{Cr}_{1-x}\text{Fe}_x)_2\text{O}_4$ for low values of x by successive replacement of Cr atoms. We have investigated the effects of sublattice occupancies and concentrations on the above mentioned properties. Our results show that the substitution of Fe at the tetrahedral sites gives rise to Co at both tetrahedral and octahedral sites, which behave very differently and produce significant effects on the structural parameters. The substantial deviation from the tetrahedral symmetry results in loss of degeneracy of the d orbitals of Fe and Co atoms occupying octahedral sites resulting in a lowering of the magnetic exchange splitting of Co atoms at octahedral positions. The inclusion of the electron electron correlation enhances the magnetic exchange splitting, thus affecting the spin states of the transition metal cations. Substitution of Fe at the octahedral site, on the other hand, does not produce such interesting effects, and the loss of symmetry of the d orbitals as a result of local structural distortion is minimal. Although at very low values of x , the substitution of Fe at B sites are energetically preferable, a tendency towards "inversion" is clearly observed with increasing x , in confirmation with experiments. The magnetic exchange interaction between Fe

atoms substituted at B sites decays exponentially with Fe-Fe distance. The antiferromagnetic exchange interactions among Fe atoms along with other magnetic species may give rise to the possibility of frustrated exchange and hence non-collinear magnetic structures. This should be investigated in detail in future.

V. ACKNOWLEDGMENTS

SG and BS acknowledge the grant from Swedish Research council VR-SIDA. DD and SG acknowledge the computation facilities from C-DAC, Pune, India and from Department of Physics, IIT Guwahati funded under the FIST programme of DST, India .

-
- * For correspondence: Biplab.Sanyal@physics.uu.se
- ¹ Y.Yamasaki, S. Miyasaka, Y. Kaneko, J.-P. He, T. Arima and Y. Torakuma, Phys. Rev. Lett. **96**, 207204 (2006).
 - ² Y.J.Choi, J.Okamoto, D.J.Huang, K.S.Chao, H.J.Lin, C.T.Chen, M.Van Veenendaal, T.A.Kaplan and S.-W.Cheong, Phys. Rev. Lett. **102**, 067601 (2009)
 - ³ K.Singh, A. Maignan, C.Simon and C. Martin, Appl. Phys. Lett. **99**, 172903 (2011)
 - ⁴ N. Menayuk, K.Dwight and A. Wold, J. Phys. France **25**, 528 (1964)
 - ⁵ K. Tomiyasu, J.Fukunaga and H.Suzuki, Phys. Rev. B **70**, 214434 (2004)
 - ⁶ L.J.Chang, D.J.Huang, W.-H.Li, S.-W.Cheong, W.Ratcliff and J.W.Lyn, J. Phys. Condens. Matt. **21**, 456008 (2009)
 - ⁷ A.V.Pronin, M.Uhlarz, R.Beyer, T.Fischer, J.Wosnitza, B.P.Gorshunov, G.A.Komandin, A.S.Prokhorov, M.Dressel, A.A.Bush and V.I.Torgashev, Phys. Rev. B **85**, 012101 (2012)
 - ⁸ V.Tsukran, S.Zherlitsyr, S.Yasin, V.Felea, Y.Skourski, J.Deisenhofer, H.A.K. Von Nidda, J.Wosnitza and A.Loidl, Phys. Rev. Lett. **110**, 115502 (2013)
 - ⁹ D.H.Lyons, T.A.Kaplan, K.Dwight and N. Menyuk, Phys. Rev. **126**, 540 (1962)
 - ¹⁰ T.H.Arima, Y.Yamasaki, T.Goto, S.Iguchi, K.Ohgushi, S.Miyasaka and Y. Tokura, J. Phys. Soc. Jpn. **76**, 023602 (2007)
 - ¹¹ C. Ederer and M. Komelj, Phys. Rev. B **76**, 064409 (2007)
 - ¹² R.Padam, S.Pandya, S.Ravi, A.K.Nigam, S.Ramakrishnan, A.K.Grover and D.Pal, Appl. Phys. Lett. **102**, 112412 (2013)
 - ¹³ R.Padam, S.Pandya, S.Ravi, A.K.Nigam, S.Ramakrishnan, A.K.Grover and D.Pal, AIP Conference Proceedings **1512**, 1112 (2013)
 - ¹⁴ W.H.Meiklejohn and C.P.Bean, Phys. Rev. **105**, 904 (1957)
 - ¹⁵ R.Padam, Ph.D. Thesis, IIT Guwahati (2014)
 - ¹⁶ H- Zhang, W-Wang, En-Liu, X-Tang, G-Li, H-Zhang and G-Wu, Phys. Stat. Solidi B **250**, 1287 (2013)
 - ¹⁷ S. Ganguly, R. Chimata and B. Sanyal, Phys. Rev. B **92**, 224417 (2015)
 - ¹⁸ P. Hohenberg and W. Kohn, Phys. Rev. B **136**, 864 (1964); W.Kohn and L.J.Sham, Phys. Rev. A **140**, 1133(1965)
 - ¹⁹ V.I.Anisimov, F.Aryasetiawan and A.I. Liechtenstein, J. Phys. Condens. Matt. **9**, 767 (1997)
 - ²⁰ I.I.Mazin and V.I.Anisimov, Phys. Rev. B **55**, 12822 (1997)
 - ²¹ Z.Fang, I.Solovyev, H.Sawada and K. Terakura, Phys. Rev. B **59**, 762 (1999)
 - ²² Z.Fang, K.Terakura, H.Sawada, T. Miyazaki and I. Solovyev, Phys. Rev. Lett. **81**, 1027 (1998)
 - ²³ D.G.Isaak, R.E.Cohen, M.J.Mehl and D.J.Singh, Phys. Rev. B **47**, 7720 (1993)
 - ²⁴ S.L.Dudarev, G.A.Botton, S.Y.Savrasov, C.J.Humphreys and A.P.Sutton, Phys. Rev. B **57**, 1505 (1998)
 - ²⁵ I.Solovyev, N.Hamada and K.Terakura, Phys. Rev. B **53**, 7158 (1996)
 - ²⁶ W.E.Pickett, S.C.Erwin and E.C.Ethridge, Phys. Rev. B **58**, 1201 (1998)
 - ²⁷ M.Cococcioni and S. de Gironcoli, Phys. Rev. B **71**, 035105 (2005)
 - ²⁸ C.J.Fennie and K.M.Rabe, Phys. Rev. B **72**, 214123 (2005)
 - ²⁹ P.E.Bloch, Phys. Rev. B **50**, 17953 (1994)
 - ³⁰ G.Kresse and J. Furthmuller, Comput. Mater. Sci. **6**, 15 (1996)
 - ³¹ J. P. Perdew, K. Burke, and M. Ernzerhof, Phys. Rev. Lett. **77**, 3865 (1996)
 - ³² G. Lawes, B.Melot, K.Page, C.Ederer, M.A.Hayward, T.Proffen and R. Seshadri, Phys. Rev. B **74**, 024413 (2006)
 - ³³ J. B. Goodenough, *Magnetism and the chemical bond*, Interscience-Wiley, New York. ISBN 0-88275-384-3 (1963).